Applied Surface Science 610 (2023) 155378

Contents lists available at ScienceDirect

Applied Surface Science

journal homepage: www.elsevier.com/locate/apsusc

Full length article

# Dynamic modeling of Si(100) thermal oxidation: Oxidation mechanisms and realistic amorphous interface generation

Lukas Cvitkovich [a,*], Dominic Waldhör [a], Al-Moatassem El-Sayed [a,b], Markus Jech [a], Christoph Wilhelmer [c], Tibor Grasser [a]

[a] Institute for Microelectronics, Technische Universität Wien, Austria
[b] Nanolayers Research Computing, Ltd., Granville Court, Granville Road, London N12 0HL, United Kingdom
[c] Christian Doppler Laboratory for Single-Defect Spectroscopy in Semiconductor Devices at the Institute for Microelectronics, Technische Universität Wien, Austria

ARTICLE INFO

*Keywords:*
Ab-initio modeling
Interface
Semiconductor
Oxidation
Atomistic modeling

ABSTRACT

Silicon and its native oxide $SiO_2$ have been utilized in semiconductor technology since the 1950s and are still crucial for the development of novel device technologies today. Recent theoretical and experimental studies show that the fabrication of high-quality interfacial layers becomes critical for reliable operation of modern nanoscale devices. This paper presents a first-principles based approach to theoretically assess the thermal oxidation process of the technologically relevant Si(100) surface in the ultra-thin layer regime below 2 nm. The oxidation process is dynamically modeled by means of ab-initio molecular dynamics and density functional based tight binding simulations. We qualitatively explain the experimentally well-known but poorly understood decrease of oxidation rate in the initial oxidation stage as a complex interplay between various oxidation mechanisms such as fast $O_2$ dissociation at the surface, slower oxygen integration mediated by molecular precursor states and $O_2$ diffusion through the oxide. Our model combines previously reported experimental insights into a comprehensive picture of Si oxide growth. Strong evidence for an immediate amorphization of the oxide surface layer was found and identified as a direct consequence of lattice vibrations. Furthermore, our modeling method is a novel approach for the generation of realistic, amorphous interface structures that is based on the stepwise oxidation of the crystalline Si surface and could be extended to other materials systems as well.

## 1. Introduction

A key requirement in micro- and nanotechnology device fabrication is the controlled production of layered material components. The semiconductor industry relies on silicon and its native oxide $SiO_2$ as a prime material system due to their well controlled manufacturing and outstanding interface properties [1]. Since recent theoretical and experimental progress enabled control of single spins confined in semiconductor nanostructures [2–4], Si is one of the prime candidates as a host material for information carriers in quantum computing and quantum spintronics [5–7]. A growing number of studies stress the importance of interface effects for such applications that can be exploited to lift undesired degeneracies and provide well defined two-state systems on the one hand [8–12], but lead to detrimental variablitites and quantum decoherence on the other [13–15]. While in modern field-effect transistors pure $SiO_2$ is gradually replaced as a gate dielectric by other materials with much higher dielectric constants [16,17] – generally referred to as high-$k$ dielectrics. However, an ultra-thin $SiO_2$ passivation layer that is grown on the Si substrate before the deposition of the high-$k$ film substantially improves the device performance [18–20] and is therefore still mandatory. Furthermore, recent fabrication and down-scaling trends shift research interests toward low-temperature chemical-based bottom-up fabrication approaches [21–23] in which the production of ultra-thin $SiO_2$ layers is of crucial importance.

$SiO_2$ layers are typically fabricated via thermal oxidation of Si. The physical mechanisms of this process have been investigated for decades, both experimentally and theoretically. Today, thicknesses of dielectric a-$SiO_2$ layers demanded for modern semiconductor technologies are in the range of a few nanometers. Thus, details of the initial oxidation stage have become more relevant in recent years and realistic atomistic interface structures are needed for improved modeling of novel device technologies. In addition, problems like the onset of amorphization of the oxide layer or the interplay between various oxidation mechanisms are still unresolved.

* Corresponding author.
*E-mail addresses:* cvitkovich@iue.tuwien.ac.at (L. Cvitkovich), grasser@iue.tuwien.ac.at (T. Grasser).

https://doi.org/10.1016/j.apsusc.2022.155378
Received 24 June 2022; Received in revised form 14 October 2022; Accepted 17 October 2022
Available online 21 October 2022

Among the various theoretical assessments of thermal oxidation, the seminal model developed by Deal and Grove accurately describes the later stages of the silicon oxidation process [24]. The model is based on the well-established concept for Si oxidation that $O_2$ molecules enter the $SiO_2$ surface layers and diffuse to the $Si/SiO_2$ interface where they dissociate and individually relax into their respective lattice sites [25–32]. However, these assumptions seem to be only valid for a well-progressed oxidation stage (oxide thickness >30 Å) as the model predictions strongly underestimate the growth rates for thin oxide films [33,34]. Massoud et al. experimentally determined the oxidation rate for thin layers and extended the Deal–Grove model by adding non-physical exponential terms in order to account for the initially enhanced growth rate [34–36]. Motivated by ab-initio calculations that suggested a strain-driven emission of Si atoms from the $Si/SiO_2$ interface, Kageshima et al. proposed a model that includes oxidation reactions within the oxide layer [37,38]. Under these assumptions, almost perfect agreement with experimental data could be achieved for oxide thicknesses >5 Å. Recent ab-initio calculations showed that the initial oxidation of a clean and reconstructed Si surface is based on chemisorption events resulting in the dissociation of the adsorbing $O_2$ molecule directly at the surface [39–41]. This was confirmed experimentally in recent electron microscopy and photoemission studies [42–44]. In addition, metastable molecular surface states were observed by means of scanning electron microscopy and electron spectroscopy techniques on thin oxide layers [44–48]. At low temperatures, these states precede dissociation events, however, vanish upon annealing. Hence, they are merely intermediate states toward the dissociative surface reaction. Both adsorption types, direct and molecular precursor mediated, were observed in molecular beam experiments [49]. According to this study, incident $O_2$ molecules of high kinetic energy (>1 eV) tend to dissociate directly, whereas the molecular precursor states originate from trapping-mediated adsorption of $O_2$ with low kinetic energy (<0.2 eV). Upon dissociation, the O atoms moved into backbonds of Si surface atoms, as correctly predicted by the aforementioned theoretical studies [39–41].

Combining these results, two major kinetic mechanisms seem to be at work: surface reactions dominate the initial stage, while the diffusion of $O_2$ becomes more important as the oxidation continues. Based on this concept, a theoretical growth model that considers dissociative chemisorption at the surface has been formulated and the resulting growth rates agree with experimental observations [50]. Further experiments indeed support the concept of two distinguishable oxidation stages. As reported in a photoelectron spectroscopy study [51], the initial stage at low $O_2$ exposure of up to 10 L (1 L: $10^{-6}$ Torr s) featured relatively rapid oxidation. Maintaining the supply of $O_2$, the oxygen surface coverage saturated and the oxidation rate was reduced as the system gradually transitioned into the Deal–Grove regime. According to transmission electron microscopy (TEM) experiments on Si nanoparticles, diffusion of $O_2$ molecules becomes important after formation of a 5 Å thick oxide layer [42].

Besides establishing the fundamental processes of oxidation, the origin of amorphization is still a controversial issue in literature. Although some studies predicted the initial growth of a crystalline Si oxide monolayers [52,53], an increase in the surface roughness during the initial oxidation was observed by atomic force microscope measurements [54] indicating an amorphous oxide growth. More recent TEM measurements support this idea and reported evidence that amorphous oxides were obtained by rapid thermal oxidation (RTO) [42,55].

In this work the initial stage of thermal oxidation of Si was studied up to an oxide thickness of 20 Å in order to investigate the growth and amorphization of ultra-thin Si oxide layers as demanded by novel devices operating on the nanoscale. Preliminary results were already published in our recent work [56]. However, the present study is far beyond and provides a comprehensive bottom-up approach focused on the thermal oxidation and its intricacies associated with its various stages. For the first time, the complete growth of an ultra-thin $SiO_2$ layer was realistically modeled within dynamic simulations in full agreement with all experimental and theoretical knowledge that has been gained on this subject until now. Earlier ab-initio studies were restricted to static calculations or used vicarious crystalline $SiO_2$ surfaces because amorphous materials could not be treated within ab-initio calculations [37,38,40,41,52,53]. The aforementioned TEM experiments only studied oxide surfaces with more than five monolayers (ML) of $SiO_2$ (from crystalline $SiO_2$: 1 ML: $6.78 \times 10^{14}$ atoms/cm$^2$ [51]). In contrast, our simulations go beyond these measurements and offer detailed insight into the oxidation process from the onset of oxidation. The thermal oxidation was modeled by the subsequent adsorption of $O_2$ molecules within ab-initio molecular dynamics (AIMD) simulations in conjunction with density functional theory (DFT). Energy barriers for the migration of oxygen in the oxide layers were obtained by nudged elastic band (NEB) calculations. The initial oxidation process featured the highest oxidation rate enabled by spontaneous surface reactions. An immediate amorphization was indicated by arbitrarily incorporated oxygen along many possible adsorption trajectories. The oxidation led to the spontaneous formation of $SiO_4$ tetrahedrons, the characteristic structural elements of a-$SiO_2$. With increasing O coverage, we observed that O-coordinated Si atoms were less susceptible for $O_2$ chemisorptions. Hence, repulsion of the incident $O_2$ became more probable and the oxidation rate decreased gradually as the surface was oxidized. In this stage, direct dissociation (<0.5 ps) was only possible for $O_2$ molecules of high kinetic energy while the molecular precursor states were typically observed for low energy molecules leading to a further decrease in the oxidation rate. The subsequent transition to the diffusion limited regime and the associated migration of $O_2$ was investigated on a 20 Å thick surface layer of a-$SiO_2$. $O_2$ diffusion became the dominate mechanism as soon as a sufficiently thick surface layer was saturated with O. The saturation was consistent with the formation of a-$SiO_2$ and indicated the transition into the Deal–Grove regime. A spontaneous dissociation, similar to the surface reaction, was then observed at the $Si/SiO_2$ interface. An overview of the mechanisms and their onset during the oxidation process is given in Fig. 1.

## 2. Methodology

Our calculations were mainly conducted at the ab-initio level utilizing density functional theory (DFT). In order to study oxidation mechanisms beyond the initial steps of O adsorption and dissociation, further investigations inevitably had to be carried out on larger model systems. Especially for DFT calculations, the computationally feasible simulation time was limited to a few ps and could be even lower for structures with an increased density of crystallographic defects. To be able to further extend our data set, we additionally used density functional based tight binding (DFTB) in conjunction with a Slater–Koster parameter set designed for Si surfaces and interfaces with $SiO_2$ [57,58]. Initial benchmarks showed that both methods yield comparable results. The details of the utilized methods and their applications within this work (cf. Fig. 1) are summarized below.

### 2.1. DFT setup

All density functional theory calculations were carried out using the CP2K package [59], a code that uses the mixed Gaussian and plane waves approach (GPW). We used a double-$\zeta$ Gaussian basis set that was optimized for condensed-phase systems consisting of Si, O, and H and the well-established Goedecker–Teter–Hutter (GTH) pseudopotentials [60,61]. The electron density was expanded using a plane-wave basis with a cutoff of 650 Ry. The exchange–correlation energy was obtained by means of the semilocal generalized gradient approximation (GGA) functional PBE. Due to its efficiency, the orbital transformation (OT) method was used by default to find the ground-state electronic structure [62]. However, within dynamic AIMD calculations, where

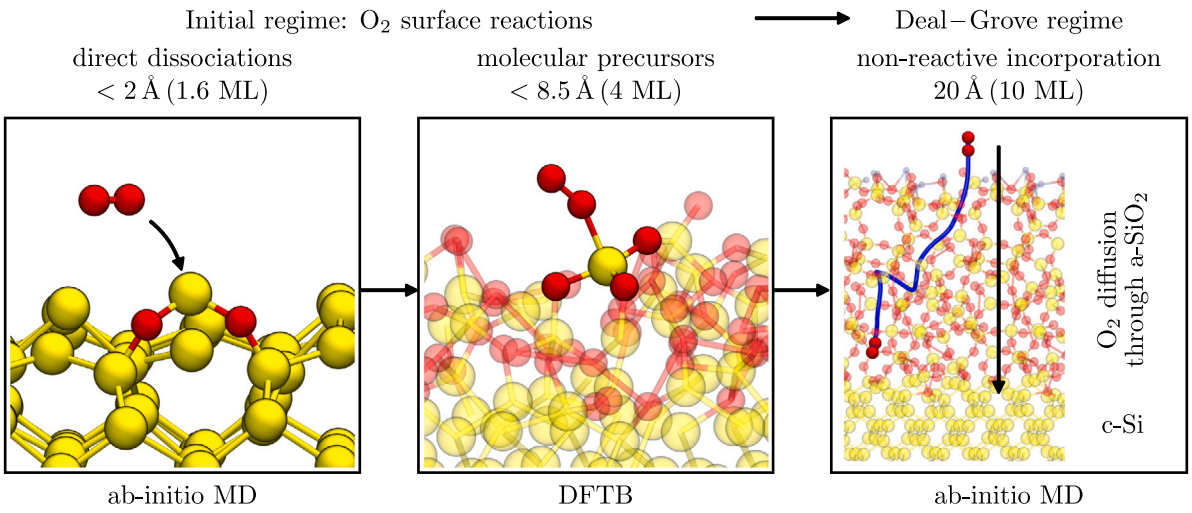


**Fig. 1.** Simulation scheme: We modeled the growth of $SiO_2$ starting from a clean Si(100) surface. In the initial stage, spontaneous and dissociative adsorptions of $O_2$ molecules were observed in DFT-based ab-initio MD (AIMD) calculations. These surface reactions are responsible for the increased growth rate compared to the Deal–Grove regime and lead to an immediate amorphization of the surface oxide. After oxidation of the first layer (oxygen coverage of 1 ML), an adsorption barrier formed and required imposing initial velocities onto the $O_2$ molecules. As soon as the oxygen coverage reached 1.6 ML, the predominant adsorption mechanism changed to a slower process exhibiting molecular $O_2$ precursors that dissociated after a few ps. In order to account for the longer simulation times needed, we employed DFTB for the further oxidation of the Si slab until a 8.5 Å oxide layer formed which showed structural characteristics of bulk a-$SiO_2$. Eventually, the saturated surface became inert to any surface reactions and $O_2$ diffusion to the Si/$SiO_2$ interface – the fingerprint of Deal–Grove oxidation – set in as observed on a 20 Å thick oxide.

several O atoms and potentially multiple unsaturated bonds were involved, Broyden's method proved to be more stable and was used instead [63]. Atomic relaxations were carried out using the Broyden–Fletcher–Goldfarb–Shanno (BFGS) algorithm [64] with a force convergence criterion of 15 meV/Å. Within the AIMD simulations, the total energy was conserved (microcanonical or NVE ensemble) and the total spin was restricted to $S = 0$. The minimal energy barrier between two configurations was calculated using the climbing-image NEB (CI-NEB) method [65,66] with a spring constant of $k = 8.2\,\mathrm{eV/Å^2}$.

### 2.2. DFTB setup

The DFTB method uses an expansion of the total energy of DFT with respect to the charge density [67]. Hamiltonian matrix elements and overlap integrals are approximated by interpolations between two-atom calculations obtained from DFT. These approximations reduce the computational costs drastically. Our DFTB simulations were carried out using the DFTB+ package [57], employing the Slater–Koster parameter set pbc-0-3 [58], which is suitable for solids and surfaces of Si–O–H systems. We considered atomic basis functions up to the s-, p- and d-shells for H, O, and Si, respectively. For geometry optimizations again the BFGS algorithm implemented in the DFTB+ package was utilized. The DFTB approach as well as the pbc-0-3 parameter set [58] are well justified as reported by a number of previous studies [68–70]. The agreement between AIMD and DFTB calculations within the scope of the present paper was ensured by a number of test calculations, e.g. the adsorption of $O_2$ molecules showed the same charge transfer of $-e$ as well as comparable reaction kinetics and adsorption configurations. Furthermore, recalculation of an AIMD trajectory reassuringly gave very similar energies. The comparative calculations are given in the supplementary material.

### 2.3. Preparation of atomic structures

The starting point of our investigations was a 4 × 4 × 12 reconstructed Si surface structure. A cleaved Si surface leads to undercoordinated Si atoms at the surface that reconstruct by forming alternating rows of tilted dimers to minimize its energy. This reconstruction reduces the number of dangling bonds on the surface via electron transfer from the lower Si dimer atom to the upper one [71]. In the present structure eight dimer pairs formed within the simulation cell. The dimers were aligned in rows that build terraces on the surface separated by cavities, the so-called channels. The dangling bonds at the bottom of the structure were passivated with hydrogen. The bottom Si layer and the passivating H atoms were fixed in AIMD runs to resemble a bulk like structure. After reconstruction of the surface, optimizing the cell including the ionic cores in the lateral directions within DFT resulted in cell dimensions of $a = b = 15.523$ Å. The cell size in the $c$-direction was set to $c = 37.22$ Å leaving a vacuum of 20 Å above the slab. The thermal oxidation of Si was studied on this model by means of AIMD until 1.6 ML of O were adsorbed. Thereafter, we employed DFTB to model the thermal oxidation up to an oxide thickness of 8.5 Å. Investigations of $O_2$ migration through the oxide were carried out on a thicker oxide model which was obtained by a melt and quench procedure [72–76] using classical molecular dynamics. Details of this procedure are given in Ref. [72]. The in this way obtained Si/$SiO_2$/Si structure was split at the oxide to generate a surface which was passivated with H and relaxed within DFT. The finished surface model consisted of a 3 × 3 × 12 Si substrate with roughly 20 Å of $SiO_2$ on top, adding up to a total of 290 atoms.

## 3. Results and discussion

A detailed picture of oxygen incorporation and amorphization at the initial stage of thermal oxidation of Si could be established from the outcome of our simulations. Our results explain the experimentally observed transition from a fast to a slow oxidation regime [42,51] by various oxygen incorporation mechanisms that supersede each other during the oxidation of only a few layers of Si. The key findings presented in this section are:

- Spontaneous surface reactions upon which the involved $O_2$ molecules dissociated.
- Immediate amorphization of the oxide layer.
- Molecular precursor states provided for a slower oxidation rate in a more progressed stage of oxidation.
- Oxygen surface saturation marked the beginning of $O_2$ diffusion through the oxide.
- Dissociation at the Si/$SiO_2$ interface due to the same charge transfer process that characterized the initial surface reactions.

### 3.1. Dynamic simulations of thermal surface oxidation

Thermal oxidation, typically in the range of 1000 K, is a highly dynamic and complex process. Previous theoretical attempts to mimic the initial stage, however, mainly relied on static calculations leading to crystalline oxide monolayers [52,53], as is also presented in the supplementary material. Therefore, accounting for lattice dynamics is a mandatory prerequisite for credible calculations. Our simulations clearly show that the various adsorption trajectories and sites strongly depend on these random movements of the involved atoms. This results in a stochastic adsorption process which ultimately prevents the growth of an ordered oxide. Our investigations on the DFT level started from the Si(100) surface with a $p(2 \times 2)$ reconstruction and ranged up to the adsorption of 13 $O_2$ molecules, corresponding to a coverage of 1.6 ML in our structures, offering insight into the amorphization of the first oxide layer. In order to study the further progression of oxidation, we employed DFTB in the following until a 8.5 Å (4 ML) thick oxide layer was obtained. We also investigated the emission of Si atoms from the interface which was suggested to be relevant in [37,38]. However, this process could not be reproduced within our simulation framework and was found to require overcoming of energy barriers in the range of 7.5 eV. Thus, this process is expected to only marginally contribute to the initial thermal oxidation process. Details on the investigations of this mechanism are given in the supplementary material.

#### 3.1.1. $O_2$ Adsorption onto the clean Si surface

Our investigations started with a single $O_2$ molecule that was placed 2.5 Å above the reconstructed Si(100) surface. An ensemble of randomly generated and Maxwell–Boltzmann (MB) distributed velocities, scaled to match the specified temperature $T = 1000$ K, was assigned to all atoms and a spin-restricted ($S = 0$) AIMD simulation with a simulation time of 3 ps and a step size of 0.5 fs was performed. Subsequently, the structure was relaxed within DFT. In this vein, several simulations with various starting configurations yielded consistent results. Fig. 2 shows snapshots of one representative $O_2$ adsorption and dissociation event together with the associated charges obtained by a Mulliken charge analysis. The $O_2$ molecule spontaneously moved toward an upper Si dimer atom that was charged positively as the $O_2$ molecule approached. After 170 fs the molecule was centered above the Si dimer atom and started to dissociate. Within the next 80 fs, the dissociation process was completed and the charges remained constant for the rest of the simulation. The two oxygen atoms relaxed into the backbonds of the upper Si dimer. In total, a charge of roughly $-e$ was transferred from the surrounding Si surface atoms to the $O_2$ molecule. In a simple molecular orbital picture, the donated electron occupied the antibonding $\pi^*$ orbital of the $O_2$ molecule, triggering its dissociation. Note that the gradual increase of charge depicted in Fig. 2 resulted from the adiabatic representation within DFT. In reality, the charge would be transferred much faster in a non-adiabatic process. Regardless, a spontaneous dissociative surface reaction was indicated by the very rapid reaction with the Si surface that was found to be independent from the starting configuration. This result was further supported by a series of static calculations. Placing $O_2$ molecules at random positions above the clean and reconfigurated Si(100) surface and relaxing the structure within DFT led to the dissociation of the molecule. Furthermore, a barrierless dissociative oxidation was also reported in [40]. Compared to the pre-adsorbed state, the intact $O_2$ molecule above the pristine Si slab, the dissociated and geometry optimized structure was 7.28 eV lower in energy. As shown in the last snapshot in Fig. 2, the Si atom on top was still undercoordinated resulting in a surface dangling bond. This exact configuration was already observed experimentally by STM images of a sparsely oxidized Si surface [44].

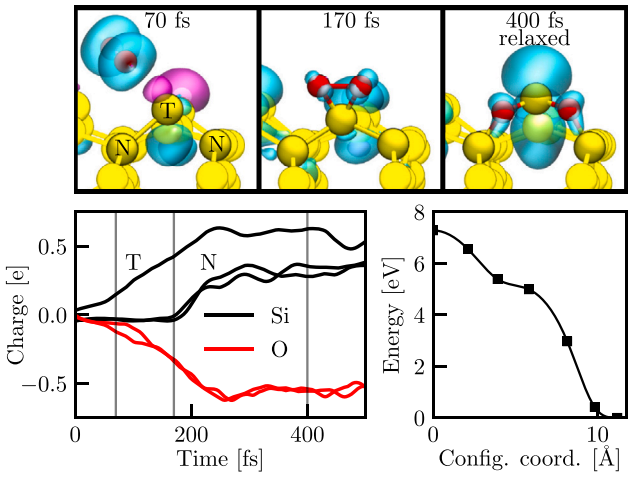


**Fig. 2.** The dissociative chemisorption of $O_2$ (red atoms) onto a clean and reconstructed Si(100) surface (yellow atoms). Snapshots of the AIMD simulation are given in the upper panel. The top right panel shows the geometry optimized structure after dissociation. The spin density for values $\pm 0.002\, e/a_0^3$ is depicted by cyan and magenta isosurfaces, respectively. The Mulliken charges of the oxygen atoms, the top dimer Si atom (T), and the neighboring Si atoms (N) during the first 500 fs of the chemisorption are shown in the lower left panel. A barrierless adsorption and dissociation is indicated by a NEB calculation along the adsorption trajectory in the lower right panel.

#### 3.1.2. Initial amorphization

Crystalline oxide structures on Si surfaces have been investigated thoroughly within theoretical studies [37,52,53] and also within this work, see the supplementary material. However, the fact that thermally grown $SiO_2$ is amorphous was established decades ago and more recent studies reported evidence that this is also true for thin films of 10 Å to 50 Å obtained by RTO, as reported by various TEM studies [42,55]. Despite these results, it is still unclear if the very first oxide layer is already amorphous. Earlier ab-initio studies were restricted to static simulations [37,52,53] while experimental studies have not looked at single oxide monolayers [42,54,55]. Within our dynamic simulations, strong evidence for immediate amorphization was found as presented in the following.

We modeled the thermal oxidation process by a series of AIMD simulations at 1000 K in which $O_2$ molecules were consecutively introduced above the reconfigurated Si(100) surface as shown in Fig. 2. The individual initial position was assigned randomly within a distance of 2 Å to 3 Å above the top Si atom. As for the adsorption in Fig. 2, the velocity was chosen randomly from a MB distribution at $T = 1000$ K. The axis of the $O_2$ molecule was aligned with the surface in order to allow for effective interaction due to larger spatial overlap between the surface dangling bonds and the oxygen $\pi^*$ orbital. The simulation time for each adsorption event was set to 1 ps. After this time, another $O_2$ molecule was introduced similarly to the previous one, while all other atoms continued to move according to their current velocity. A Mulliken charge analysis showed that the fundamental oxidation mechanism – a dissociative chemisorption via a charge transfer similar to the reaction shown in Fig. 2 – underlay every single adsorption during the initial surface oxidation. However, adsorption became less probable as the oxidation progressed. Only the first six adsorptions, corresponding to an oxygen coverage of 0.7 ML in our structures, happened spontaneously. After that, the $O_2$ molecules were occasionally repelled from already oxidized Si atoms. In this case, the run was discarded. After 9 successful adsorptions (or 1.1 ML), a spontaneous adsorption could not be observed within 10 runs. We interpreted the decrease in adsorption probability as the emergence and subsequent increase of an adsorption barrier with proceeding oxidation. In order to overcome the formed adsorption barrier and to study further oxidation within a reasonable time frame, we imposed an initial velocity of 1000 m/s toward the

surface for the $O_2$ molecule from this point onward. This value roughly complies with the average velocity of $\overline{v} = 810\,\mathrm{m/s}$ according to the MB distribution of non interacting $O_2$ molecules at $T = 1000\,\mathrm{K}$. Adsorption of $O_2$ – a process that happened spontaneously onto the clean surface within static and dynamic calculations – was inhibited by the oxide formation on the surface. This behavior qualitatively explained the decrease of the oxidation rate measured in the initial stage of oxidation [51] and gave rise to the non-reactive $O_2$ diffusion process later on [24].

The immediate amorphization of the oxide layer is enabled by a stochastic adsorption process in which the adsorption trajectory of each $O_2$ molecule depends strongly on its initial position and velocity and even on fluctuations of the surface lattice due to thermal vibrations. The stochastic character of the oxidation process is indicated by many different adsorption trajectories featuring comparable energy gains and strongly varying final configurations. Representative adsorption trajectories of three successive runs are given in the supplementary material.

The adsorption trajectories were very sensitive to changes of the environment as investigated by two comparative AIMD runs. As shown in Fig. 3, the adsorption of an $O_2$ molecule was sampled for two different velocity distributions (taken from a MB distribution as described above) of the surface lattice. The initial position and velocity of the $O_2$ molecule was identical for both runs. The resulting trajectories are completely different although the energy gain of around 6.5 eV is very similar. This implies that even weak perturbations alter the resulting structure substantially. Note that the respective trajectories are not important and would look completely different for any ensemble of initial velocities. Hence, Fig. 3 illustrates the large effect of slightest changes in initial conditions. The intrinsic high degree of randomness during the oxidation provides strong evidence for the immediate amorphization of the oxide layer.

### 3.1.3. Molecular precursors

Sampling slower surface reactions and more spontaneous adsorptions in which the adsorption barrier was overcome, requires a longer simulation time together with an increased number of calculations. Furthermore, extending our investigations in the direction of the formation of a-$SiO_2$ required a larger amount of oxygen. Hence, we conducted these calculations within DFTB. The molecules were placed about 2 to 3 Å above a surface Si atom before MD simulations of 10 ps with a step size of 0.5 fs were conducted. The first simulation started with random initial velocities (MB distribution at $T = 1000$ K) for all surface atoms that were passed on to the subsequent run. The $O_2$ velocities were sampled from the same distribution though restricted to the negative $z$-direction. If a molecule was repelled from the surface, it was removed from the simulation cell at the end of the run.

After the first Si layer was oxidized, spontaneous dissociative adsorptions could hardly be observed. Instead, the $O_2$ molecules adsorbed via a metastable molecular precursor state. Dissociation events of these molecules could be sampled within the time-extended DFTB simulations, as shown in Fig. 4. Again, the dissociation was induced by a charge transfer. The surface was subjected to a considerable reconfiguration, mainly associated with the breakage of multiple Si–O bonds adjust for the dissociation and incorporation in a $SiO_4$ tetrahedron. Such precursor states block further adsorption of oxygen molecules and thus effectively lower the rate of oxidation. As mentioned above, we also observed the direct adsorption and dissociation mechanism, provided the $O_2$ molecules possess a sufficiently high kinetic energy, see the supplemental material. However, this process required $O_2$ velocities from the top one percent of the MB distribution and was thus ranked negligible in the framework of this work. However, both mechanisms involve the breaking of bonds between already dissociated O atoms and neighboring Si which is only feasible if the O atoms find new positions, i.e. can bind to Si atoms below that are not fully oxidized yet. Thus, the rate for direct dissociative oxidation gradually decreases as the oxidation advances and eventually can be considered negligible once a few layers of Si are oxidized. The precursor-mediated process with a reduced oxidation rate is dominant in this regime.

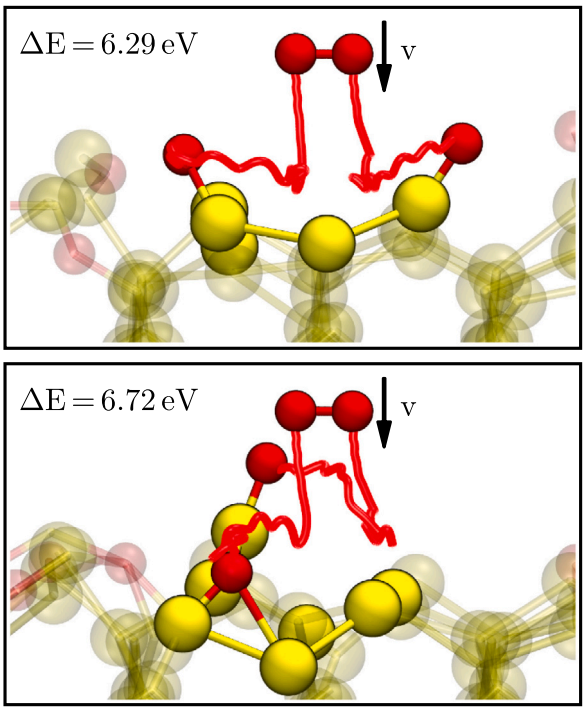


**Fig. 3.** Two examples of $O_2$ adsorption trajectories of $O_2$ adsorptions with the same initial position and velocity of the $O_2$ molecule but different velocities for the surface atoms. The velocities of the lattice atoms were randomly sampled from a Maxwell–Boltzmann distribution at 1000 K. The snapshots show the final positions after a simulation time of 450 fs superimposed with the starting configuration. Also shown are the trajectories of the adsorbing O atoms (red lines). The energy gains $\Delta E$ were calculated for geometry optimized structures.

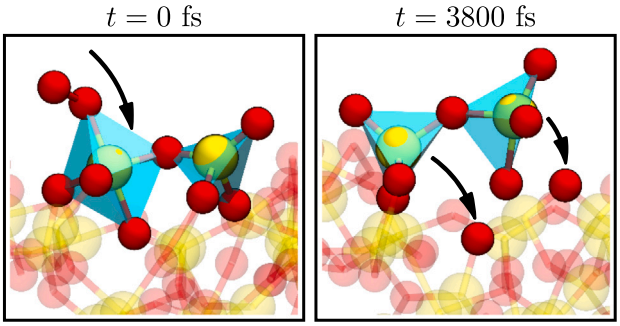


**Fig. 4.** Molecular precursor states. The $O_2$ molecule adsorbs to a already fully oxidized Si atom (the $SiO_4$ tetrahedron is indicated by blue planes) and stays in the vicinity of this atom for around 4 ps within our simulations until it finally dissociates. Two O atoms migrate to lower Si atoms adjusting for the incorporation of the dissociated O atoms, as indicated by the black arrows.

## 3.2. Surface saturation

The oxide layer reached a total thickness of 8.5 Å after the adsorption of 32 $O_2$ molecules or 4 ML. As presented in the following section, the oxide could be subdivided into a 3.5 Å thick layer of a-$SiO_2$ on top of a 5 Å transition region. In this stage, all Si atoms on the surface were fully O coordinated and incorporated in a spontaneously formed $SiO_4$ tetrahedron, see Figs. 4 and 5. As a result, the surface structure was highly unordered. A spontaneous adsorption of $O_2$ molecules onto this surface could not be observed, as an additional molecule was repelled from 25 random positions. The chemical composition of the a-$SiO_2$ surface layer was $SiO_{1.95}$. A structural analysis of this layer showed that the bond lengths and angles are already comparable to the experimentally obtained values for bulk a-$SiO_2$ [77,78]: the average

Si–O distance was 1.66 Å and the binding angles showed an average of 108° for O-Si–O and 132.5° for Si–O–Si, see Fig. 5. The slightly larger bond lengths (compared to 1.62 Å of bulk $SiO_2$) could be assigned to surface effects. The O–Si–O angles matched the perfect tetrahedral bond angle of 109.47°. The Si–O–Si angle averaged at 132.5°, which agreed well with the conclusions reached in Ref. [79], that the angle is reduced to 135° in thin films compared to 148° in bulk structures. Furthermore, the Si–O–Si angles were broadly distributed between 100° to 160° which indicated a vitreous (amorphous) form of silica. The density of the $SiO_2$ layer was roughly 2.33 g/cm$^3$ in agreement with measured values [77]. The density of the transition layer directly at the Si/$SiO_2$ interface was slightly increased to values up to 2.7 g/cm$^3$ which agrees with an intrinsic compressive stress as reported in [80–82]. A Mulliken charge analysis allowed us to infer the oxidation state of each Si. Due to the strong electronegativity of O, a Si–O bond is represented by an increase of the Si's associated Mulliken charge. As determined by a reference calculation in defect-free a-$SiO_2$, the fully oxidized state $Si^{4+}$ corresponded to an increase of roughly 1$e$ in our DFT setup, yielding ~ 0.3$e$ of excess charge on the Si ion per Si–O bond. The prevalence of different Si oxidation states as determined by this relation during the thermal oxidation is shown in the middle panel in Fig. 5. For a sparsely oxidized surface, the O was distributed evenly on the Si atoms as shown by the large number of $Si^+$. In later stages however, most Si were fully O coordinated with only a few partially O-coordinated Si atoms that were located at the interface to the Si substrate. $Si^{4+}$ atoms were fully coordinated by O and incorporated in a $SiO_4$ tetrahedron. We observed that the transition into the $O_2$ diffusion regime (Deal–Grove regime) happened as soon as a sufficiently thick surface layer was fully oxidized. In this stage, the $O_2$ could not chemically react with the surface anymore and thus diffusion of $O_2$ through the oxide set in.

### 3.3. Si/$SiO_2$ interface

Within computational material modeling, the construction of credible interface structures between amorphous oxides and crystalline substrates is a challenging task [83,84]. Typically, computationally modeled Si/$SiO_2$ interfaces are created using a melt and quench procedure [72–76]. In this approach, atomistic structures are melted at temperatures of up to 7000 K within simulation times of tens of picoseconds while ensuring that the silicon maintains its crystalline structure and the oxygen is confined to a certain region.

Many previous DFT studies have relied on crystalline interfaces between Si and quartz $SiO_2$ because amorphous interfaces could not be treated within first-principles calculations [37,38,40,41,52]. In contrast, by consecutively adsorbing $O_2$ molecules onto the Si surface in dynamic simulations, we naturally obtained a credible interface between the amorphous oxide and the crystalline Si substrate. When using the melt and quench method, on the other hand, a very low defect density can be achieved. Even entirely defect-free configurations can be generated using this method [72,73]. The stepwise oxidation on the other hand gave interfaces that show larger stresses, a higher degree of disorder and a larger probability to generate defects (e.g. over/undercoordinated atoms), see the comparison in Fig. 6. However, a reliable quantitative comparison of defect densities cannot be given within the scope of this work since the simulation time of our AIMD/DFTB calculations lies far away from those of classical MD simulations and thus did not allow for possible reconfiguration of the amorphous surface layer.

In order to investigate oxidation states at the interface, we plotted the Mulliken charges of the Si atoms vs. the corresponding $z$-position, as shown in Fig. 6 (c). Note that the oxidation state +1 that is associated with one Si–O bond corresponds to a charge transfer of 0.3$e$ in the Mulliken charge analysis. All Si atoms in the surface $SiO_2$ layer were fully oxidized and their associated Mulliken charge was increased by $e$. The transition region was about 5 Å thick and could be identified via intermediate charge states of the silicon atoms. The linear transition

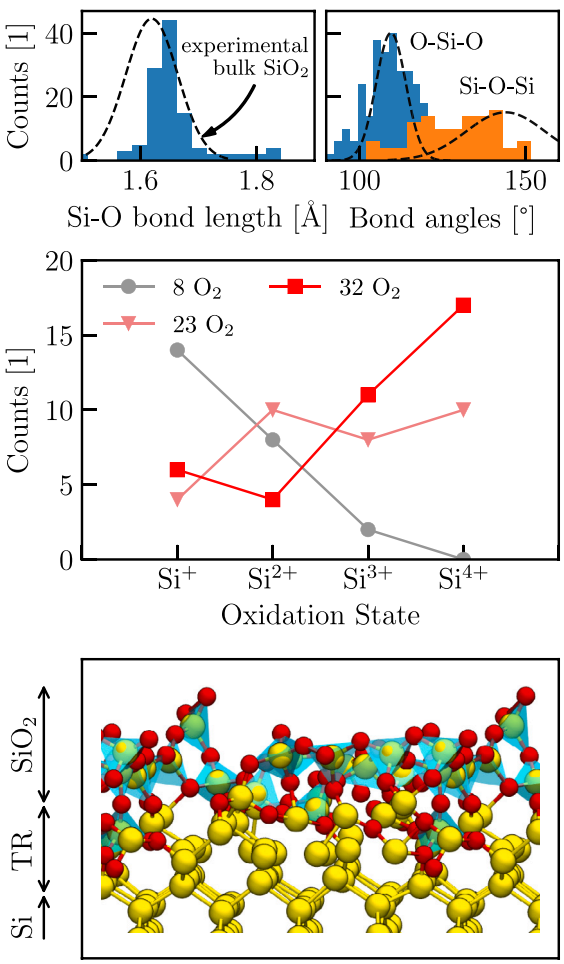


**Fig. 5.** Characteristics of the $SiO_2$ growth obtained by dynamic simulations within DFTB. Distributions of the bond lengths and angles and the comparison to experimental values of bulk $SiO_2$ [77,78] (dashed lines) are shown in the top panel. The prevalence of different Si oxidation states as obtained by a Mulliken charge analysis is shown in the middle panel. As oxidation continues, the amount of $Si^{4+}$ (fully oxidized Si atoms that are incorporated in $SiO_4$ tetrahedrons) increases whereas the amount of $Si^+$ converges to a lower value that represents states in the transition region (TR) between the oxide and the crystalline Si substrate. The final and geometry optimized structure is shown in the lower panel. $SiO_4$ tetrahedrons on the immediate surface are indicated by blue planes.

of associated charges in the transition region was also found in structures obtained by the melt and quench method. Such interface regions between crystalline Si and the amorphous oxide with a thickness of 5 Å to 7 Å were indicated by TEM images [77] and electron-energy-loss spectroscopy [85] (EELS) measurements. In agreement with previous studies that reported an intrinsic stress of 0.3 – 0.8 GPa around the interface [80–82], we observed stretched bonds in our stepwise oxidized interfaces near the oxidation front that could exceed typical Si–Si bond lengths by about 5% even for correctly coordinated Si atoms and elongated Si–O bonds that were increased by up to 12%. Ultimately, this led to Si tetrahedrons with asymmetric charge distributions which altered the assigned Mulliken charge. Hence, only a rough assignment of oxidation states in the transition region was attainable. In particular, the decrease of the charge of some Si atoms in the transition region was considered to be an artifact of these lattice distortions. These outliers were specific to the stepwise oxidation method and can thus be considered as another indication for larger stresses in the obtained structure.

In the following section, we show that the weakened interface bonds represent preferred places for the dissociation of $O_2$ molecules. As

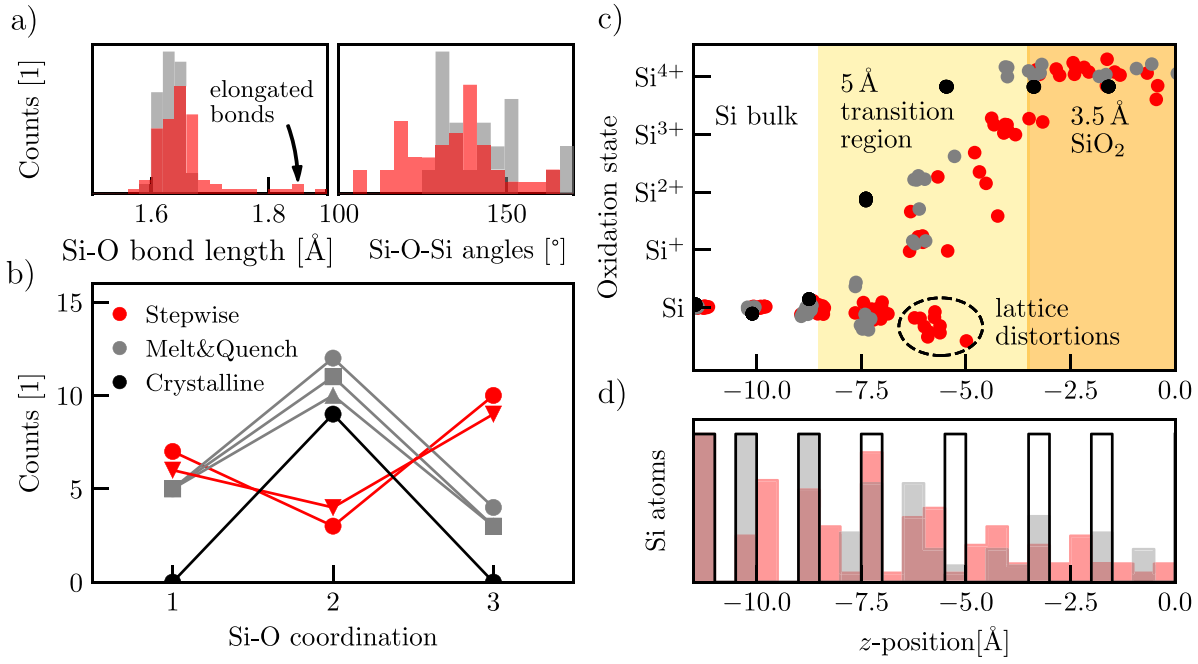


**Fig. 6.** Comparison between interfaces obtained via various modeling techniques: the stepwise oxidation approach from this work (red) is compared to the melt and quench method [72] (gray) and to ad-hoc crystalline Si-quartz interfaces (black). (a) Distribution of bond lengths and angles around the interface. The stepwise generated interface shows bonds that are elongated by up to 12% and strongly distorted Si–O–Si angles that indicate large strain. (b) O-coordination of Si atoms near the interface. The melt and quench method produced mostly two-fold O-coordinated Si reminiscent of crystalline interfaces. In contrast, the stepwise approach yields higher coordinated Si atoms. (c) Oxidation states as obtained by a Mulliken charge analysis of Si atoms vs. their respective $z$-position. Amorphous $SiO_2$ is indicated by fully oxidized Si atoms (oxidation state +4). The oxidation states in the roughly 5 Å thick transition region can only be assigned approximately. The stepwise oxidation method shows negative oxidation states that are indicative of strong lattice distortions. (d) Distribution of Si atoms vs. their respective $z$-position. The stepwise approach inherently yields a broader distribution indicating a larger degree of disorder compared to the melt and quench approach in which non-oxidized Si atoms are artificially fixed during the MD calculation. A number of interfaces were compared, however, for the sake of perceptibility only one representative configuration is shown in (a), (c) and (d) as the results were very similar for each method.

discussed above, O–Si–O angles in the oxide above the transition region matched the perfect tetrahedral bond angle of 109.47°, indicating that these tetrahedrons were not distorted. Thus, the Mulliken charge could be assigned quite accurately in these cases. In contrast, Si–O–Si angles close to our novel interface structures are widely distributed. Again, this indicates large strains close to the interface since these angles represent the orientation between individual $SiO_4$ tetrahedrons and can in general be more easily distorted.

Summarizing the above results, the stepwise oxidation method yielded interface structures with a larger degree of randomness compared to the melt and quench technique. The dynamic oxidation inherently served as an approach which allowed for unconstrained generation of credible, realistic interfaces. The corresponding structures are available upon request [86].

### 3.4. Oxygen migration

Another important aspect of the surface oxidation process is the migration of incorporated oxygen. First, we examined the possibilities of thermal diffusion of already adsorbed single O atoms by calculating energy barriers for the migration in Si bulk and from the surface oxide into deeper layers of the Si surface. Large diffusion barriers suggest that this mechanism is not important for the oxide growth. In contrary, in later stages of the oxidation process, i.e. after a layer of about 5 to 10 Å of a-$SiO_2$ formed on the surface, oxygen is incorporated by diffusion of $O_2$ molecules through the amorphous oxide, as assumed within the Deal–Grove model. We investigated this mechanism by AIMD simulations and confirmed the assumptions of Deal and Grove, namely, that oxygen molecules enter the oxide non-reactively and dissociate spontaneously when reaching the $Si/SiO_2$ interface. Larger oxide models were used for these simulations since the interface of our DFTB obtained structure (see Fig. 5) is still close to the surface and thus allows for the dissociative incorporation of molecular precursors as described above.

#### 3.4.1. Migration of adsorbed O atoms

To obtain diffusion barriers for single O atom migration in a bulk Si system we first calculated the energy barrier for the migration of one single O atom in a Si bulk material. As verified within geometry optimizations, the energetically favored positions of an O atom incorporated in a Si crystal are the Si bond center sites [87]. Utilizing NEB calculations, we obtained the minimum energy path between two neighboring bond center sites. The energy barrier of 1.72 eV in our pristine Si crystal agrees with other theoretical studies of O migration in Si [88–90]. With this result the experimentally derived energy barrier of 2.5 eV [91] can be obtained by considering a coupled-barrier diffusion [92]. In order to derive an estimate for the rate of the process at $T = 1000$ K we employed the Arrhenius equation with an attempt frequency of $6 \times 10^{12}\,s^{-1}$ [93] and the 1.72 eV barrier yielding $9 \times 10^{4}\,s^{-1}$. Enlarged barriers were found for O migration from the surface oxide structures obtained by our AIMD simulations, see Fig. 7. We specifically investigated diffusion in the transition region between the crystalline and amorphous structures since it offered alternative positions for O atoms. Two examples of possible diffusion paths for one O atom were calculated and yielded energy barriers of at least 2.8 eV, or a reaction rate of $4 \times 10^{-4}\,s^{-1}$. Keeping the experimental oxidation growth rate of about 1 Å/s [94] for the initial stage of thermal oxidation of Si in mind, only a small contribution to the overall growth rate by thermal migration of single O atoms is expected. However, migration of O atoms is required for the dissociation of molecular precursors and thus still plays an important role in the oxidation process. The observation of slow oxygen migration in the amorphous surface layers together with an increased adsorption barrier explains the decrease of oxidation rate as the oxidation proceeds. In this manner, the oxide growth rate decreases gradually as the dominant oxidation mechanism transitions from spontaneous surface reactions to precursor reactions and finally into the non-reactive $O_2$ diffusion regime.

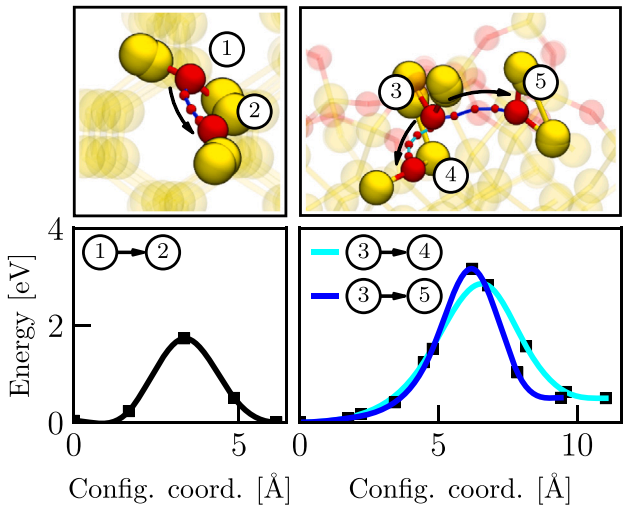


**Fig. 7.** Energy barriers for thermal diffusion of O in Si bulk (left) and from a surface oxide layer (right) as obtained by NEB calculations. The trajectories of the diffusion are indicated by solid blue and cyan lines in the top panels and the resulting energy barriers are shown in the respective lower panels. Intermediate configurations along the trajectories are depicted as smaller O atoms. The results show that thermal diffusion of O from the oxidized surface layers is strongly inhibited compared to the diffusion in Si bulk and would only contribute marginally to the overall oxidation process that is almost exclusively driven by $O_2$ diffusion through the oxide.

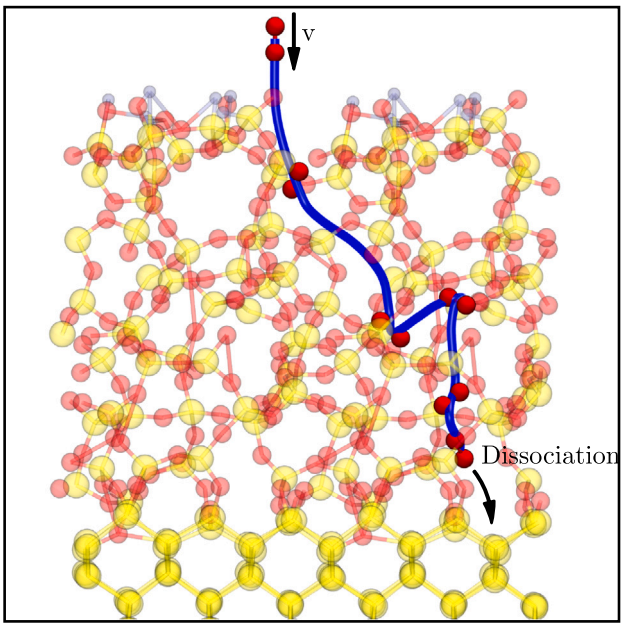


**Fig. 8.** Diffusion of $O_2$ in a-$SiO_2$ is enabled for thicker oxide layers. The non-reactive incorporation and migration through the oxide layer is shown by the results of an AIMD simulation with a simulation time of 3 ps. An initial velocity of 800 m/s was assigned to the $O_2$ molecule. The trajectory of the center of mass of the molecule is depicted by a solid blue line. The molecule eventually reaches the Si/$SiO_2$ interface and dissociates, see Fig. 9.

### 3.4.2. $O_2$ Diffusion through the oxide

Diffusion of $O_2$ through thicker oxide layers during thermal oxidation as proposed by [24] was well investigated in other studies [25–32,95–97]. The diffusion barrier was found to be extremely sensitive to the local structural topology which is reflected by a wide spread of DFT calculated values from 0.5 eV to 2.8 eV [27,95]. Experimentally, values between 0.7 and 1.6 eV [97] were found for oxide films produced in various ways. Our own NEB calculations of $O_2$ diffusion processes agree nicely with previous theoretical and experimental results and yielded barriers between 0.7 and 2 eV. Hence, molecular stability as well as sufficient diffusibility of $O_2$ in silicon dioxide can be safely assumed also within the framework of our calculations.

We observed the non-reactive incorporation of $O_2$ molecules on a 20 Å thick oxide layer that was obtained by a melt and quench procedure [72]. As shown in Fig. 8, a seamless migration through the oxide could be sampled in an AIMD simulation with a simulation time of 3 ps. The molecules' initial velocity was set to 800 m/s. Without interaction, the $O_2$ entered the oxidized surface and migrated along a random path determined by deflections at the $SiO_2$ structure. This result specifically indicates that further oxidation now mainly occurs at the buried interface, which will in return remain qualitatively unchanged as the reaction principles comply with the Deal–Grove assumptions.

### 3.4.3. $O_2$ Dissociation at the interface

In the $O_2$ diffusion regime, further oxidation of the Si substrate occurs at the buried Si/$SiO_2$ interface upon dissociation of the $O_2$ molecule [24]. From a macroscopic point of view, $O_2$ migration yields an oxidation front that moves from the surface deeper into the substrate. This process could be confirmed within our simulations by another set of AIMD calculations.

An $O_2$ molecule was placed above the transition region between the amorphous oxide and its crystalline substrate. Due to lattice distortions, some Si atoms in the transition region possess strained bonds or even dangling bonds, cf. Fig. 6. These dangling bonds are known to affect the reliability of semiconductor devices and are therefore usually passivated with H after the oxidation [72,98]. However, the simulations showed that these atoms were the preferred dissociation spots. The initial velocity of the $O_2$ molecule was set to zero in order to verify the feasibility of a spontaneous reaction. As shown in Fig. 9, the $O_2$ molecule spontaneously dissociates via essentially the same charge transfer process as in the dissociative chemisorption at the Si surface, cf. Fig. 2. In addition, further evidence for a barrierless dissociation was obtained by another NEB calculation. Here, $O_2$ was placed above the transition region in order to include a short diffusion path of 4 Å preceding the actual dissociation. The migration toward the strained bond was governed by a comparably low diffusion barrier of 0.2 eV. In Fig. 9, the beginning of the dissociative process is indicated by a strong decrease of the potential energy surface. The large energy gain of 9.4 eV could be justified by a complex reconfiguration at the interface in which multiple bonds with considerable binding energies break (O–O: 2.1 eV; Si–Si: 4.9 eV) and form (Si–O: 6.5 eV). Additionally, the molecular configuration contained the incorporation energy of the oxygen molecule in the oxide layer which was evaluated to be 0.4 eV in bulk $SiO_2$ by DFT calculations [99]. In this stage, the oxide growth rate is not limited by the supply of oxygen to the surface anymore but by the $O_2$ diffusion rate through the oxide and is thus certainly much slower compared to the initial oxidation, as assumed within the Deal–Grove model [24].

## 4. Conclusions

We modeled the oxidation of a Si(100) surface by means of ab-initio DFT and the closely related DFTB simulation techniques and obtained credible surface models of ultra thin native oxide layers on a Si substrate. For the first time, the highly complex thermal oxidation process could be consistently reproduced for ultra-thin $SiO_2$ layers (<5 Å) within simulations that reveal an oxidation scheme which combines all experimental observations that have been reported on this subject up to now such as surface reactions, adsorption into molecular precursor states and $O_2$ diffusion through the oxide [24–32,39–44,44–49,51,55].

Starting from the clean $p(2\times2)$ reconstructed Si surface we gradually introduced molecular oxygen into the system by adding $O_2$ molecules above the surface. In this manner, we dynamically modeled the $O_2$

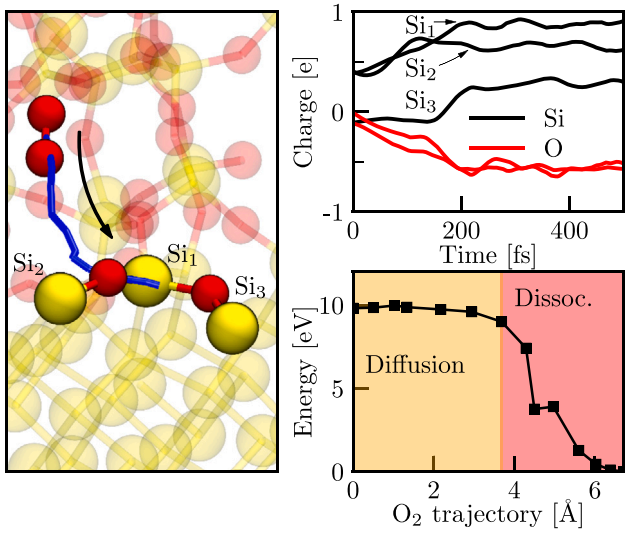


**Fig. 9.** $O_2$ dissociation at the $Si/SiO_2$ interface. The left panel shows the trajectory of the center of mass of the $O_2$ molecule (solid blue line) together with the initial (molecular) and final (dissociated) configurations of the NEB calculation. The Mulliken charges for the spontaneous dissociation as captured within an AIMD simulation are depicted in the top right panel. The Mulliken analysis reveals another charge transfer of $-e$ that strongly resembles the dissociative reactions at the surface during the initial stage of oxidation, cf. Fig. 2. The associated charges of the $Si_1$ and $Si_2$ atoms show an offset due to the implications of the interface, cf. Fig. 6. The potential energy surface of this process is displayed in the lower right panel and indicates diffusion along a 4 Å long trajectory that is only inhibited by a low barrier of 0.2 eV. In addition to the AIMD results, the NEB calculation provides evidence for a spontaneous dissociation as soon as the molecule reached the dissociation spot.

chemisorption until a 3.5 Å thick $SiO_2$ layer formed above a 5 Å transition region. Immediate amorphization from the onset of oxidation was indicated by a stochastic adsorption processes in which many barrierless adsorption trajectories with similar energy gains of around 6 eV led to strongly varying final positions. The amorphization was thus demonstrated to be a direct consequence of lattice vibrations. The top a-$SiO_2$ layer showed many characteristics of bulk $SiO_2$ such as geometric measures (bond angles and lengths) and density already for thicknesses of ∼3.5 Å. Furthermore, it was recognized by the oxidation states of the Si atoms, which is +4 for fully oxidized Si atoms incorporated in $SiO_4$ tetrahedrons, the building blocks of bulk $SiO_2$. The oxide layer was separated from the crystalline Si substrate by a 5 Å thick transition layer.

In the initial oxidation stage, the adsorption of $O_2$ was a spontaneous process and directly followed by the dissociation of the molecule upon which the O atoms moved into Si–Si bond center sites. Thus, this stage features the fastest oxidation rate that is only limited by the supply of oxygen. Further oxidation of an already partly oxidized Si surface atom was found to require overcoming of an adsorption barrier. Therefore, after oxidation of the first Si layer, the molecules were occasionally repelled and direct dissociation could only be observed for molecules with kinetic energies from the top one percent of the Maxwell–Boltzmann distribution. However, the adsorption of $O_2$ molecules into molecular precursor states that only dissociated after some picoseconds was commonly monitored in longer MD runs. The slower dissociation mechanism and the decreased adsorption probability led to an overall decrease of the oxide growth rate. Finally, the oxide layer became thick enough to effectively block any surface reactions leading to the dissociation of the $O_2$ molecule. Now the diffusion of $O_2$ through the oxide to the $Si/SiO_2$ interface – as assumed within the Deal–Grove model – set in. As soon as the $O_2$ molecule reached the $Si/SiO_2$ transition layer with a substantial amount of strained configurations, it again spontaneously dissociated via a charge transfer reaction that strongly resembled the surface reactions during the initial stage of oxidation. Consequently, further oxidation occurs mainly at the buried interface, which will in return remain qualitatively unchanged as the reaction principles stay consistent during the rest of the oxidation process. Thus, our simulational approach can be utilized for generating realistic, amorphous interface structures that might be applied to other material systems as well. Compared to the standard melt and quench technique, our stepwise oxidation method respects more realistic conditions of thermal oxidation and yields highly disordered interfaces that are subjected to a significant inherent stress as indicated by strained bonds, compressed angles and an increased density.

Based on the qualitative behavior of the oxidation process, estimates for the transition into the diffusive Deal–Grove regime can be given. Direct surface reactions dominate only during oxidation of the first and second Si layer (oxide thickness ∼4 Å). Subsequently, in an intermediate stage, molecular precursor states provide for a slower oxidation until a layer of a-$SiO_2$ has formed above the ∼5 Å transition region. Starting from 10 Å total oxide thickness, the surface should be inert to any surface reactions and thus allow for the diffusion of molecular oxygen within the a-$SiO_2$ layer.

## CRediT authorship contribution statement

**Lukas Cvitkovich:** Main author, Conducted simulations and result analysis. **Dominic Waldhör:** Advisory function. **Al-Moatassem El-Sayed:** Advisory function. **Markus Jech:** Creator of melt and quench interfaces, Advisory function. **Christoph Wilhelmer:** Advisory function. **Tibor Grasser:** Advisory function.

## Declaration of competing interest

The authors declare that they have no known competing financial interests or personal relationships that could have appeared to influence the work reported in this paper.

## Data availability

Resulting interface structures are available upon request [86]

## Acknowledgments

This project has received funding from the European Union's Horizon 2020 research and innovation programme under grant agreement No. 871813, within the framework of the project Modeling Unconventional Nanoscaled Device FABrication (MUNDFAB), Austria. Furthermore, the financial support by the Austrian Federal Ministry for Digital and Economic Affairs and the National Foundation for Research, Technology and Development, Austria and from the Vienna Scientific Cluster (VSC), Austria is gratefully acknowledged.

## Appendix A. Supplementary data

Supplementary material related to this article can be found online at https://doi.org/10.1016/j.apsusc.2022.155378.

## References

[1] M. Razeghi, Technology of Quantum Devices, first ed., Springer US, 2010, pp. 41–82, Chapter 2.
[2] A. Chatterjee, P. Stevenson, S. De Franceschi, Nat. Rev. Phys. 3 (2021) 157–177, http://dx.doi.org/10.1038/s42254-021-00283-9.
[3] G. Burkard, T.D. Ladd, J.M. Nichol, A. Pan, J.R. Petta, https://arxiv.org/abs/2112.08863. http://dx.doi.org/10.48550/ARXIV.2112.08863.
[4] P. Stano, D. Loss, Nat. Rev. Phys. 4 (2022) 672–688, http://dx.doi.org/10.1038/s42254-022-00484-w.
[5] M. Fogarty, K. Chan, B. Hensen, et al., Nature Commun. 9 (2018) 4370, http://dx.doi.org/10.1038/s41467-018-06039-x.
[6] R. Zhao, T. Tanttu, T. K.Y., et al., Nature Commun. 10 (2019) 5500, http://dx.doi.org/10.1038/s41467-019-13416-7.

[7] J. Yoneda, W. Huang, M. Feng, et al., Nature Commun. 12 (2021) 4114, http://dx.doi.org/10.1038/s41467-021-24371-7.
[8] L.E. Golub, E.L. Ivchenko, Phys. Rev. B 69 (2004) 115333.
[9] M.O. Nestoklon, L.E. Golub, E.L. Ivchenko, Phys. Rev. B 73 (2006) 235334.
[10] J.K. Gamble, M.A. Eriksson, S.N. Coppersmith, M. Friesen, Phys. Rev. B 88 (2013) 035310.
[11] L. Bourdet, Y.-M. Niquet, Phys. Rev. B 97 (2018) 155433.
[12] F.A. Zwanenburg, A.S. Dzurak, A. Morello, M.Y. Simmons, L.C.L. Hollenberg, G. Klimeck, S. Rogge, S.N. Coppersmith, M.A. Eriksson, Rev. Modern Phys. 85 (2013) 961–1019.
[13] D. Deith, S.K. Gorman, Y. He, et al., NPJ Quantum Inf. 8 (2022) 17, http://dx.doi.org/10.1038/s41534-022-00523-5.
[14] C. Spence, B. Cardoso-Paz, V. Michal, et al., 2022, http://dx.doi.org/10.48550/ARXIV.2209.01853, https://arxiv.org/abs/2209.01853.
[15] B. Martinez, Y.-M. Niquet, Phys. Rev. Appl. 17 (2022) 024022, https://link.aps.org/doi/10.1103/PhysRevApplied.17.024022.
[16] M.M. Waldrop, Nature 530 (2016) 144–147, http://dx.doi.org/10.1038/530144a.
[17] Y. Illarionov, T. Knobloch, T. Grasser, Nat. Electron. 3 (2020) 442–443, http://dx.doi.org/10.1038/s41928-020-0464-2.
[18] R. de Almeida, I. Baumvol, Surf. Sci. Rep. 49 (1) (2003) 1–114, http://dx.doi.org/10.1016/S0167-5729(02)00113-9.
[19] C. Mahata, I.-K. Oh, C.M. Yoon, C.W. Lee, J. Seo, H. Algadi, M.-H. Sheen, Y.-W. Kim, H. Kim, T. Lee, J. Mater. Chem. C 3 (2015) 10293–10301, http://dx.doi.org/10.1039/C5TC01890K.
[20] A. Nakajima, Q.D. Khosru, T. Yoshimoto, S. Yokoyama, Microelectron. Reliab. 42 (12) (2002) 1823–1835, http://dx.doi.org/10.1016/S0026-2714(02)00095-1.
[21] O. Nur, M. Willander, in: O. Nur, M. Willander (Eds.), Low Temperature Chemical Nanofabrication, in: Micro and Nano Technologies, William Andrew Publishing, 2020, pp. 87–147, http://dx.doi.org/10.1016/B978-0-12-813345-3.00004-6.
[22] Q. Yao, X. Ma, H. Wang, Y. Wang, G. Wang, J. Zhang, W. Liu, X. Wang, J. Yan, Y. Li, W. Wang, Nanomaterials 11 (4) (2021) 955, http://dx.doi.org/10.3390/nano11040955.
[23] C. Krzeminski, G. Larrieu, J. Penaud, E. Lampin, E. Dubois, J. Appl. Phys. 101 (6) (2007) 064908, http://dx.doi.org/10.1063/1.2711764.
[24] B.E. Deal, A.S. Grove, J. Appl. Phys. 36 (12) (1965) 3770–3778, http://dx.doi.org/10.1063/1.1713945.
[25] A. Bongiorno, A. Pasquarello, J. Mater. Sci. 40 (2005) 3047–3050, http://dx.doi.org/10.1007/s10853-005-2663-7.
[26] A. Bongiorno, A. Pasquarello, Phys. Rev. Lett. 93 (2004) 086102, http://dx.doi.org/10.1103/PhysRevLett.93.086102.
[27] A. Bongiorno, A. Pasquarello, Phys. Rev. B 70 (2004) 195312, http://dx.doi.org/10.1103/PhysRevB.70.195312.
[28] A. Pasquarello, M.S. Hybertsen, R. Car, Nature 396 (6706) (1998) 58–60, http://infoscience.epfl.ch/record/141662.
[29] F.J. Himpsel, F.R. McFeely, A. Taleb-Ibrahimi, J.A. Yarmoff, G. Hollinger, Phys. Rev. B 38 (1988) 6084–6096, https://link.aps.org/doi/10.1103/PhysRevB.38.6084.
[30] T. Akiyama, H. Kageshima, Surf. Sci. 576 (1) (2005) L65–L70, http://dx.doi.org/10.1016/j.susc.2005.01.001.
[31] E.P. Gusev, H.C. Lu, T. Gustafsson, E. Garfunkel, Phys. Rev. B 52 (1995) 1759–1775, https://link.aps.org/doi/10.1103/PhysRevB.52.1759.
[32] E. Rosencher, A. Straboni, S. Rigo, G. Amsel, Appl. Phys. Lett. 34 (4) (1979) 254–256, http://dx.doi.org/10.1063/1.90771.
[33] M.A. Hopper, R.A. Clarke, L. Young, J. Electrochem. Soc. 122 (9) (1975) 1216–1222, http://dx.doi.org/10.1149/1.2134428.
[34] H.Z. Massoud, J.D. Plummer, E.A. Irene, J. Electrochem. Soc. 132 (11) (1985) 2685–2693, http://dx.doi.org/10.1149/1.2113648.
[35] H.Z. Massoud, J.D. Plummer, E.A. Irene, J. Electrochem. Soc. 132 (11) (1985) 2693–2700, http://dx.doi.org/10.1149/1.2113649.
[36] H.Z. Massoud, J.D. Plummer, J. Appl. Phys. 62 (8) (1987) 3416–3423, http://dx.doi.org/10.1063/1.339305.
[37] H. Kageshima, K. Shiraishi, Phys. Rev. Lett. 81 (1998) 5936–5939, http://dx.doi.org/10.1103/PhysRevLett.81.5936.
[38] H. Kageshima, K. Shiraishi, M. Uematsu, Japan. J. Appl. Phys. 38 (Part 2, No. 9A/B) (1999) L971–L974, http://dx.doi.org/10.1143/jjap.38.l971.
[39] L.C. Ciacchi, M.C. Payne, Phys. Rev. Lett. 95 (2005) 196101, http://dx.doi.org/10.1103/PhysRevLett.95.196101.
[40] K. Kato, T. Uda, Phys. Rev. B 62 (2000) 15978–15988, https://link.aps.org/doi/10.1103/PhysRevB.62.15978.
[41] C.-Y. Niu, J.-T. Wang, J. Chem. Phys. 139 (2013) 194709, http://dx.doi.org/10.1063/1.4832340.
[42] Y.-C. Liao, A.M. Nienow, J.T. Roberts, J. Phys. Chem. B 110 (12) (2006) 6190–6197, http://dx.doi.org/10.1021/jp054195e.
[43] A. Yoshigoe, Y. Yamada, R. Taga, S. Ogawa, Y. Takakuwa, Japan. J. Appl. Phys. 55 (10) (2016) 100307, http://dx.doi.org/10.7567/jjap.55.100307.
[44] D. Kaya, R.J. Cobley, R.E. Palmer, Nano Res 13 (2020) 145–150, http://dx.doi.org/10.1007/s12274-019-2587-1.
[45] E. Hwang, Y.H. Chang, Y.-S. Kim, J.-Y. Koo, H. Kim, J. Korean Phys. Soc. 61 (7) (2012) 1046–1050, http://dx.doi.org/10.3938/jkps.61.1046.
[46] U. Höfer, P. Morgen, W. Wurth, E. Umbach, Phys. Rev. B 40 (1989) 1130–1145, http://dx.doi.org/10.1103/PhysRevB.40.1130.
[47] B.A. Ferguson, C.T. Reeves, C.B. Mullins, J. Chem. Phys. 110 (23) (1999) 11574–11584, http://dx.doi.org/10.1063/1.478005.
[48] P. Morgen, U. Höfer, W. Wurth, E. Umbach, Phys. Rev. B 39 (1989) 3720–3734, http://dx.doi.org/10.1103/PhysRevB.39.3720.
[49] B.A. Ferguson, C.T. Reeves, C.B. Mullins, J. Chem. Phys. 110 (23) (1999) 11574–11584, http://dx.doi.org/10.1063/1.478005.
[50] T.K. Whidden, P. Thanikasalam, M.J. Rack, D.K. Ferry, J. Vac. Sci. Technol. B 13 (4) (1995) 1618–1625, https://avs.scitation.org/doi/abs/10.1116/1.587867.
[51] Y. Hoshino, T. Nishimura, T. Nakada, H. Namba, Y. Kido, Surf. Sci. 488 (3) (2001) 249–255, http://dx.doi.org/10.1016/S0039-6028(01)01165-7.
[52] F. Fuchs, W.G. Schmidt, F. Bechstedt, Phys. Rev. B 72 (2005) 075353, https://link.aps.org/doi/10.1103/PhysRevB.72.075353.
[53] N. Salles, N. Richard, N. Mousseau, A. Hemeryck, J. Chem. Phys. 147 (5) (2017) 054701, http://dx.doi.org/10.1063/1.4996206.
[54] K. Ohsawa, Y. Hayashi, R. Hasunuma, K. Yamabe, J. Phys. Conf. Ser. 191 (2009) 012031, http://dx.doi.org/10.1088/1742-6596/191/1/012031.
[55] P. Mur, M. Semeria, M. Olivier, A. Papon, C. Leroux, G. Reimbold, P. Gentile, N. Magnea, T. Baron, R. Clerc, G. Ghibaudo, Appl. Surf. Sci. 175–176 (2001) 726–733, http://dx.doi.org/10.1016/S0169-4332(01)00081-2, 10th International Conference on Solid Films and Surfaces.
[56] L. Cvitkovich, M. Jech, D. Waldhör, A.-M. El-Sayed, C. Wilhelmer, T. Grasser, ESSDERC 2021 - IEEE 51st European Solid-State Device Research Conference (ESSDERC), 2021, pp. 235–238, http://dx.doi.org/10.1109/ESSDERC53440.2021.9631790.
[57] B. Aradi, B. Hourahine, T. Frauenheim, J. Phys. Chem. A 111 (26) (2007) 5678–5684, http://dx.doi.org/10.1021/jp070186p, PMID: 17567110.
[58] C. Köhler, Z. Hajnal, P. Deák, T. Frauenheim, S. Suhai, Phys. Rev. B 64 (2001) 085333, http://dx.doi.org/10.1103/PhysRevB.64.085333.
[59] J. VandeVondele, M. Krack, F. Mohamed, M. Parrinello, T. Chassaing, J. Hutter, Comput. Phys. Comm. 167 (2) (2005) 103–128, http://dx.doi.org/10.1016/j.cpc.2004.12.014.
[60] J. VandeVondele, J. Hutter, J. Chem. Phys. 127 (11) (2007) 114105, http://dx.doi.org/10.1063/1.2770708.
[61] S. Goedecker, M. Teter, J. Hutter, Phys. Rev. B 54 (1996) 1703–1710, http://dx.doi.org/10.1103/PhysRevB.54.1703.
[62] J. VandeVondele, J. Hutter, J. Chem. Phys. 118 (10) (2003) 4365–4369, http://dx.doi.org/10.1063/1.1543154.
[63] C.G. Broyden, IMA J. Appl. Math. 6 (3) (1970) 222–231, http://dx.doi.org/10.1093/imamat/6.3.222.
[64] D. Goldfarb, Math. Comp. 24 (109) (1970) 23–26, https://doi.org/10.1090/S0025-5718-1970-0258249-6.
[65] R. Elber, M. Karplus, Chem. Phys. Lett. 139 (5) (1987) 375–380, http://dx.doi.org/10.1016/0009-2614(87)80576-6.
[66] G. Henkelman, B.P. Uberuaga, H. Jónsson, J. Chem. Phys. 113 (22) (2000) 9901–9904, http://dx.doi.org/10.1063/1.1329672.
[67] M. Elstner, D. Porezag, G. Jungnickel, J. Elsner, M. Haugk, T. Frauenheim, S. Suhai, G. Seifert, Phys. Rev. B 58 (1998) 7260–7268, http://dx.doi.org/10.1103/PhysRevB.58.7260.
[68] G. Zheng, S. Irle, K. Morokuma, Chem. Phys. Lett. 412 (1) (2005) 210–216, http://dx.doi.org/10.1016/j.cplett.2005.06.105.
[69] N. Capel, D. Bharania, S. Manzhos, Computation 3 (4) (2015) 574–585, http://dx.doi.org/10.3390/computation3040574.
[70] T. Qi, C.W. Bauschlicher, J.W. Lawson, T.G. Desai, E.J. Reed, A. Lenfant, J. Phys. Chem. A 118 (28) (2014) 5355–5357, http://dx.doi.org/10.1021/jp505594b.
[71] A. Ramstad, G. Brocks, P.J. Kelly, Phys. Rev. B 51 (1995) 14504–14523, http://dx.doi.org/10.1103/PhysRevB.51.14504.
[72] M. Jech, A.-M. El-Sayed, S. Tyaginov, A.L. Shluger, T. Grasser, Phys. Rev. B 100 (2019) 195302, http://dx.doi.org/10.1103/PhysRevB.100.195302.
[73] A.-M. El-Sayed, M.B. Watkins, V.V. Afanas'ev, A.L. Shluger, Phys. Rev. B 89 (2014) 125201, https://link.aps.org/doi/10.1103/PhysRevB.89.125201.
[74] S. Mukhopadhyay, P.V. Sushko, A.M. Stoneham, A.L. Shluger, Phys. Rev. B 70 (2004) 195203, https://link.aps.org/doi/10.1103/PhysRevB.70.195203.
[75] Y. Wang, F. Zahid, J. Wang, H. Guo, Phys. Rev. B 85 (2012) 224110, https://link.aps.org/doi/10.1103/PhysRevB.85.224110.
[76] A. de Jamblinne de Meux, G. Pourtois, J. Genoe, P. Heremans, J. Phys. D: Appl. Phys. 48 (43) (2015) 435104, http://dx.doi.org/10.1088/0022-3727/48/43/435104.
[77] A.C. Diebold, D. Venables, Y. Chabal, D. Muller, M. Weldon, E. Garfunkel, Mater. Sci. Semicond. Process. 2 (2) (1999) 103–147, http://dx.doi.org/10.1016/S1369-8001(99)00009-8.
[78] R.L. Mozzi, B.E. Warren, J. Appl. Crystallogr. 2 (4) (1969) 164–172, http://dx.doi.org/10.1107/S0021889869006868.
[79] K. Hirose, H. Nohira, T. Koike, K. Sakano, T. Hattori, Phys. Rev. B 59 (1999) 5617–5621, http://dx.doi.org/10.1103/PhysRevB.59.5617.
[80] R.J. Jaccodine, W.A. Schlegel, J. Appl. Phys. 37 (6) (1966) 2429–2434, http://dx.doi.org/10.1063/1.1708831.
[81] E.P. EerNisse, Appl. Phys. Lett. 35 (1) (1979) 8–10, http://dx.doi.org/10.1063/1.90905.

[82] E. Kobeda, E.A. Irene, J. Vac. Sci. Technol. 5 (1) (1987) 15–19, https://avs.scitation.org/doi/abs/10.1116/1.583853.
[83] S. Ling, A.-M. El-Sayed, F. Lopez-Gejo, M.B. Watkins, V. Afanas'ev, A.L. Shluger, Microelectron. Eng. 109 (2013) 310–313, http://dx.doi.org/10.1016/j.mee.2013.03.028.
[84] U. Khalilov, E.C. Neyts, G. Pourtois, A.C.T. van Duin, J. Phys. Chem. C 115 (50) (2011) 24839–24848, http://dx.doi.org/10.1021/jp2082566.
[85] D.A. Muller, T. Sorsch, S. Moccio, F.H. Baumann, K. Evans-Lutterodt, G. Timp, Nature 399 (6738) (1999) 758–761, http://dx.doi.org/10.1038/21602.
[86] Please contact cvitkovich@iue.tuwien.ac.at or grasser@iue.tuwien.ac.at.
[87] W. Bond, W. Kaiser, J. Phys. Chem. Solids 16 (1) (1960) 44–45, http://dx.doi.org/10.1016/0022-3697(60)90069-X.
[88] M. Needels, J. Joannopoulos, Y. Bar-Yam, S. Pantelides, R. Wolfe, MRS Proceedings 209 (1990) 103, http://dx.doi.org/10.1557/PROC-209-103.
[89] M. Saito, A. Oshiyama, Phys. Rev. B 38 (1988) 10711–10717, http://dx.doi.org/10.1103/PhysRevB.38.10711.
[90] P.J. Kelly, R. Car, Phys. Rev. B 45 (1992) 6543–6563, http://dx.doi.org/10.1103/PhysRevB.45.6543.
[91] S.-T. Lee, D. Nichols, Appl. Phys. Lett. 47 (9) (1985) 1001–1003, http://dx.doi.org/10.1063/1.95969.
[92] M. Ramamoorthy, S.T. Pantelides, Phys. Rev. Lett. 76 (1996) 267–270, https://link.aps.org/doi/10.1103/PhysRevLett.76.267.
[93] J. Koettgen, T. Zacherle, S. Grieshammer, M. Martin, Phys. Chem. Chem. Phys. 19 (2017) 9957–9973, http://dx.doi.org/10.1039/C6CP04802A.
[94] T. Hoshino, Y. Nishioka, Phys. Rev. Lett. 84 (2000) 4633–4636, http://dx.doi.org/10.1103/PhysRevLett.84.4633.
[95] T. Bakos, S.N. Rashkeev, S.T. Pantelides, Phys. Rev. Lett. 88 5 (2002) 055508, http://dx.doi.org/10.1103/PHYSREVLETT.88.055508.
[96] T. Hoshino, M. Hata, S. Neya, Y. Nishioka, T. Watanabe, K. Tatsumura, I. Ohdomari, Japan. J. Appl. Phys. 42 (Part 1, No. 6A) (2003) 3560–3565, http://dx.doi.org/10.1143/jjap.42.3560.
[97] J. Perez-Bueno, R. Ramirez-Bon, Y. Vorobiev, F. Espinoza-Beltran, J. Gonzalez-Hernandez, Thin Solid Films 379 (1) (2000) 57–63, http://dx.doi.org/10.1016/S0040-6090(00)01568-6.
[98] S. Pantelides, S. Wang, A. Franceschetti, R. Buczko, M. Vetra, S. Rashkeev, L. Tsetseris, M. Evans, I.G. Bartyrev, Mater. Sci. Forum 527–529 (2006) 935–948, http://dx.doi.org/10.4028/www.scientific.net/msf.527-529.935.
[99] A.M. Stoneham, M.A. Szymanski, A.L. Shluger, Phys. Rev. B 63 (2001) 241304, http://dx.doi.org/10.1103/PhysRevB.63.241304.